Mon. Not. R. Astron. Soc. (2005) doi:10.1111/j.1365-2966.2005.09535.x

# Can variability account for apparent age spreads in OB association colour–magnitude diagrams?

Ben Burningham,[1⋆] Tim Naylor,[1] S. P. Littlefair[1,2] and R. D. Jeffries[3]

[1]*School of Physics, University of Exeter, Stocker Road, Exeter EX4 4QL*
[2]*Department of Physics and Astronomy, University of Sheffield, Sheffield S3 7RH*
[3]*Department of Physics, Keele University, Keele, Staffordshire ST5 5BG*

Accepted 2005 August 17. Received 2005 August 5; in original form 2005 May 17

**ABSTRACT**

We have investigated the role of photometric variability in causing the apparent age spreads observed in the colour–magnitude diagrams of OB associations. We have found that the combination of binarity, photometric uncertainty and variability on time-scales of a few years is not sufficient to explain the observed spread in either of the OB associations we have studied. Such effects can account for about half the observed spread in the $\sigma$ Orionis subgroup and about 1/20 of the observed spread in Cep OB3b. This rules out variability caused by stellar rotation and rotation of structures within inner accretion discs as the source of the majority of the apparent age spreads. We also find that the variability tends to move objects parallel to isochrones in $V/V - i'$ colour–magnitude diagrams (CMDs), and thus has little influence on apparent age spreads. We conclude that the remaining unexplained spread either reflects a true spread in the ages of the pre-main-sequence (PMS) objects or arises as a result of longer term variability associated with changes in accretion flow.

**Key words:** stars: formation – stars: low-mass, brown dwarfs – stars: pre-main-sequence – stars: variables: other – open clusters and associations: individual: $\sigma$ Orionis – open clusters and associations: individual: Cep OB3b.

## 1 INTRODUCTION

A significant unresolved question in the study of star formation is how long it takes. Whether we are considering the entire process from the state of neutral interstellar hydrogen to the zero-age main-sequence, or just the portion of the process from the fragmentation of a giant molecular cloud (GMC) onwards, there is no consensus as to how long star formation takes. There are two competing paradigms of star formation currently proposed in the literature, which each give rise to very different time-scales for star formation.

### 1.1 Slow star formation

Shu (1977) put forward the model of star formation which we will refer to as slow star formation (SSF), which was reviewed by Shu, Adams & Lizano (1987). In this model, molecular cloud complexes are in dynamical equilibrium, with lifetimes of several tens of megayears and are supported against free-fall collapse by magnetic fields. However, in clumps where the density is $n \gtrsim 10^5\,\mathrm{cm}^{-3}$, the ionization fraction can be sufficiently low that the neutral molecular material may diffuse through the magnetic field, removing flux from the core (ambipolar diffusion), leading to higher degrees of central condensation. Eventually, the field can no longer support the, now prestellar, core against gravitational collapse to form a hydrostatic protostar.

Typically, predicted ambipolar diffusion time-scales lie in the range 5–10 Myr. This is consistent with the observed lifetimes of pre-stellar cores with $10^5 < n < 10^6$ found by Ward-Thompson et al. (1994) to be $\sim 10^6$ yr, through comparison of the number of starless cores versus protostellar cores. However, Jijina, Myers & Adams (1999) performed a more comprehensive study of pre-stellar cores using ammonia emission. They found the ratio of starless to stellar cores to be too small to be consistent with that expected if the ambipolar diffusion time-scale governed core lifetimes. This suggests that the time-scale of the starless core phase is much less than the ambipolar diffusion time-scale.

### 1.2 Rapid star formation

More recently, an alternative paradigm for pre-stellar core formation and collapse has been discussed in the literature (e.g. Ballesteros-Paredes, Hartmann & Vázquez-Semadeni 1999; Elmegreen 2000; Hartmann 2001; Hartmann, Ballesteros-Paredes & Bergin 2001). In this model, the star formation rate is regulated by supersonic turbulence, not by magnetic fields. Since supersonic turbulence in self-gravitating clouds is expected to decay rapidly, the cloud support mechanism in this picture leads to a short cloud lifetime compared

⋆E-mail: bgb@astro.ex.ac.uk

to that in SSF (Pringle, Allen & Lubow 2001). Therefore, rather than being long-lived structures, GMCs are treated as transient objects that form through interactions between supersonic flows in the interstellar medium. The whole process from the formation of the GMCs through to the arrival of the pre-main-sequence (PMS) stars on the birthline is expected to take around 3 Myr, with collapse of cores to form protostars occurring almost immediately. As such we will refer to this model as rapid star formation (RSF). RSF has a number of distinct advantages over SSF, both observationally and theoretically, which are reviewed by Mac Low & Klessen (2004).

### 1.3 Age spreads

The presence of apparent age spreads has been observed in a number of young clusters (e.g. Herbst & Miller 1982; Sung, Bessell & Lee 1998) and associations (e.g. Dolan & Mathieu 2001; Pozzo et al. 2003), and their sizes have been presented as evidence in favour of both SSF and RSF. Palla & Stahler (2000) investigated apparent age spreads in a number of young star-forming regions and found evidence of accelerating star formation, which they use to argue in favour of SSF. A further study by the same authors of the age spread in the Taurus–Auriga region also found evidence of accelerating star formation (Palla & Stahler 2002). The evidence of accelerating star formation in the regions studied by these authors came in the form of distributions of stellar ages that were, generally, strongly peaked at 1–2 Myr, with few PMS stars older than this. As Hartmann (2003) pointed out, this surely implies that there is something special about the last 1–2 Myr, if such widely separated regions have formed the majority of their stars at the same time, whilst their overall lifetimes are $\sim$10 Myr. Such an uncomfortable, special, state of affairs is not required if one accepts the RSF paradigm. This is because the strong peaking of age distributions at 1–2 Myr follows naturally if this is the time-scale for cloud and star formation (Hartmann 2003).

Elmegreen (2000) found that the age spreads seen in a number of OB associations and clusters are comparable to the inferred crossing time for the parent cloud. The conclusion that is drawn from this is that the age spread is indicative of the time-scale for star formation, and that this is comparable to the crossing time, as expected for RSF. However, his data reveal that the age spreads also scale with the mean ages for the groups he uses. This scaling of apparent age spreads with mean age for clusters and associations suggests that the age spreads originate from a photometric scatter of given magnitude. The size of this spread is much larger than any photometric uncertainties. Since PMS objects move more slowly through colour–magnitude space at older ages, a given photometric scatter will naturally imply larger age spread as the mean age rises. The correlation of spread with inferred crossing time may also arise as a result of the fact that older open clusters and associations are larger and thus a longer crossing time is inferred for the parent cloud.

Hartmann (2001, 2003) disputed the results and conclusions of Palla & Stahler (2000, 2002), arguing that the actual age spreads are much smaller than those observed, but accepted that the presence of such large age spreads ($10^7$ yr) would be a problem for the RSF paradigm. Additionally, it is not clear that the interpretation of the age spreads being indicative of time-scale is correct. Tassis & Mouschovias (2004) pointed out that the interpretation of age spreads in this manner already assumes a core formation time-scale that is essentially instantaneous with respect to the lifetime of the molecular cloud, $\tau_{\rm mc}$. In reality, an age spread could only tell us the difference between $\tau_{\rm mc}$ and the time-scale for forming a body that will survive the destruction of the molecular cloud, the core formation time-scale, $\tau_{\rm cf}$. Therefore $\tau_{\rm spread} = \tau_{\rm mc} - \tau_{\rm cf}$. As such, interpretation of any spread in ages is dependent on the knowledge of either $\tau_{\rm cf}$ or $\tau_{\rm mc}$.

Incidentally, this point is also relevant to the argument put forward by Hartmann et al. (2001) that, since very few young clusters or associations older than 3 Myr are associated with their parent cloud, star formation must occur on a time-scale of about 3 Myr. This also implicitly assumes that $\tau_{\rm cf}$ is short. The same observational evidence could indicate that star formation is slow, but that the cloud is disrupted quickly after the first PMS stars arrive at the birthline. However, as pointed out by Hartmann et al. (2001), the vast majority of local molecular cloud complexes show evidence of star formation. This must imply that $\tau_{\rm cf}$ should be short, or the question must surely be asked as to the whereabouts of the clouds which are still mostly in the pre-stellar phase of star formation. This is reflected in the results of Jijina et al. (1999), described earlier, that the ratios of pre-stellar to stellar cores found in molecular clouds are far below the 3 to 30:1 range required by SSF.

It is important to recognize, however, that the reality of apparent age spreads has not been well established. The principal evidence for spreads of ages actually comes from an observed spread of PMS stars in colour–magnitude (C–M) space. A single age would be expected to give rise to a much more narrow distribution of stars about an isochrone. There are a number of plausible alternatives that could explain such C–M spreads for a population that in reality arrived at the birthline simultaneously. For example, accretion-driven age spread (Tout, Livio & Bonnell 1999) could give rise to an apparent spread of ages for an ensemble of objects with differing accretion histories. Hartmann (2001) explored a number of other factors that might be expected to influence the degree of observed age spread. These included variable extinction, photometric variability, differences in accretion luminosities and the presence of unresolved binaries. Establishing the influence of variability and binarity on the width of the PMS in OB association-like environments is the aim of this work. We have obtained two-epoch, two-colour photometry for two regions with differing photometric spreads to investigate this effect. The two regions studied here are within well-known OB associations: Cep OB3b and the $\sigma$ Orionis (Ori) young group (part of the Orion OB1b association). We have simulated the degree of spread introduced by variability on time-scales of less than 1 yr in Cep OB3b and less than 4 yr in $\sigma$ Ori. By comparing two-colour catalogues of PMS objects within these associations, we have estimated their variability, and used this to simulate the PMS in the C–M space, assuming a single isochronal age for the objects.

The rest of the paper is laid out as follows. In Section 2, we describe our observations and data reduction. In Section 3, we describe how we have simulated the spreads in each of our associations in turn, and give the basic results. These results are discussed in Section 4, and our conclusions are summarized in Section 5.

## 2 OBSERVATIONS AND DATA REDUCTION

All observations were carried out using the Wide Field Camera (WFC) mounted on the Isaac Newton Telescope (INT) at the Roque de los Muchachos Observatory, La Palma. Our first epoch data set for $\sigma$ Ori is the same as that presented by Kenyon et al. (2005). It was made up of observations taken on the nights of 1999 September 27–30 of five fields of view (FOV) in the Harris $R$ and Sloan $i'$ filters. We carried out observations of four FOVs coincident with Kenyon et al.'s survey on the night of 2003 September 7, using the same filters. The new observations are detailed in Table 1. We have obtained new data for both epochs for our Cep OB3b survey. We have observed a single WFC FOV in this region, chosen to cover

**Table 1.** Summary of observations.

| Field name | $\sigma$ Ori 1 | | $\sigma$ Ori 2 | | $\sigma$ Ori 3 | | $\sigma$ Ori 4 | | Cep OB3b | |
|---|---|---|---|---|---|---|---|---|---|---|
| RA (J2000) | 054014.2 | | 05 40 13.1 | | 053807.7 | | 05 38 07.4 | | 225543.3 | |
| Dec. (J2000) | −022018.1 | | −025148.0 | | −02 20 18.0 | | −025151.0 | | +62 40 13.7 | |
| Filter | *R* | $i'$ | *R* | $i'$ | *R* | $i'$ | *R* | $i'$ | *V* | $i'$ |
| 2003-09-07 | 600 s | 300 s | 600 s | 300 s | 600 s | 300 s | 600 s | 300 s | – | – |
| 2003-09-12 | – | – | – | – | – | – | – | – | 30 s, 2 s | 13 s, 2 s |
| 2004-09-28 | – | – | – | – | – | – | – | – | 30 s, 5 s | 300 s, 30 s, 5 s |

the area with the highest density of PMS objects identified by Pozzo et al. (2003). Observations were taken on the nights of 2003 September 12 and 2004 September 28 using Harris *V* and Sloan $i'$ filters. The observations are detailed in Table 1.

Data obtained in 2003 and 2004 were reduced in an identical manner. Flat-fields and data frames were linearized using the 2003 August coefficients (see http://www.ast.cam.ac.uk/∼wfcsur/technical/foibles/index.php for details), and then bias-subtracted using a median bias frame specific to each night. We flat-fielded the data using frames constructed from twilight sky flat-fields taken during the same observing runs as the data being corrected. The $i'$-band frames were successfully defringed using a fringe frame from 2001 September, obtained from the web pages of the Cambridge Astronomy Survey Unit (CASU).

Optimal photometry was performed using the method laid out by Naylor (1998) and Naylor et al. (2002), with the revisions described in Burningham et al. (2003) and Littlefair et al. (2005). We have allowed the profile correction to vary with position on each chip, and fitted it with a third-order polynomial in the *x*-axis and a fifth-order polynomial in the *y*-axis. We do not apply the 'ill-determined sky' flag for the Cep OB3b data, and we allow the thresholds for its application to vary from field to field for the $\sigma$ Ori data. For obvious reasons, we did not apply the 'variable' data quality flag to reject objects that showed evidence of variability. An astrometric solution was obtained through comparison with a 2MASS catalogue for each FOV. The rms of the residuals to the six-coefficient fits was all less than 0.1 arcsec.

As described by Naylor et al. (2002), overlap regions between pointings were used to normalize the catalogues for each pointing on to a single system. We use the same method to bring observations from two epochs for each of our target regions to the same system. In the case of the $\sigma$ Ori data, the way in which flat-fields were normalized had changed between the two epochs, so the data from each epoch were treated slightly differently. When the 1999 data were reduced, the flat-field for each chip on the WFC was normalized separately. By the time the 2003 data were reduced, the reduction software had been changed such that the flat-fields for all the four chips in each pointing were normalized together. As such, prior to catalogue normalization, the 1999 exposures were combined to produce one catalogue for each chip, whilst the 2003 exposures were combined to produce one catalogue for each pointing. The overlap regions between the interlocking pointings were then used to normalize the catalogues on to a single system.

To verify that there were no major sources of error introduced at the image processing stage, we checked that the distribution of positive and negative differences between observations was uniform with position on the sky for the $\sigma$ Ori data. We found that the trends in the differences between observations were correlated with the pixel coordinates on each chip from the first epoch catalogue. Kenyon et al. (2005) found the rms of differences between overlap stars seen in their data to be 0.05 mag and speculated that it was due to problems with the flat-field, which is consistent with what has been seen here. They state that the camera was suffering from light leaks during their observing run, and it is likely that this is the origin of the problem. We fitted the trends in the differences in *x* and *y* for each chip with first- and second-order polynomial functions, and corrected the magnitudes of the objects in the first epoch catalogue accordingly, prior to renormalizing the two epochs. The rms of the differences in the magnitudes in the interlocking overlap regions after normalization suggested that an additional magnitude-independent uncertainty of about 0.01 mag was also present. As in Naylor et al. (2002), this uncertainty was included in the uncertainty estimate for all objects. Following this, we found that the positive and negative differences for the $\sigma$ Ori data were spatially uncorrelated.

Since no overlap regions were present in the Cep OB3b data sets, we could not use the results of the normalization to determine the size of any additional uncertainty, so we applied the same value as found for the $\sigma$ Ori data set. The distribution of positive and negative differences was found to be spatially uncorrelated in the Cep OB3b data set.

We have not applied a measured photometric calibration to our final catalogues as this would have involved transforming our Harris and Sloan magnitudes and colours into the Cousins system. Such a transformation would risk introducing spurious correlations between variability and colour, whilst not improving our experiment in any way. As such, we have simply applied mean zero-points to our magnitudes and colour coefficients to our colours to construct our CMDs.

## 3 SIMULATION OF PHOTOMETRIC SPREADS

### 3.1 The $\sigma$ Ori subgroup

The $\sigma$ Ori young group has been the subject of a number of spectroscopic studies aimed at identifying bona fide members. In particular, two campaigns (Burningham et al. 2005; Kenyon et al. 2005) were successful in identifying a large number of members present in the catalogue obtained from the first epoch observations. Importantly, these spectroscopic surveys also demonstrated that photometric selection of the PMS objects in this region is not subject to serious contamination, and does not miss significant numbers of bona fide members. As such, we have used the membership lists from these studies to define a PMS region in the CMD, with minimal contamination, from which we have drawn our sample (see Fig. 1). Only objects with little doubt as to their membership have been used to guide the photometric selection. In the case of the Burningham et al. (2005) catalogue, this meant objects with greater than 90 per cent membership velocity probability. In the case of the Kenyon et al. (2005) catalogue, this meant objects that displayed strong Li

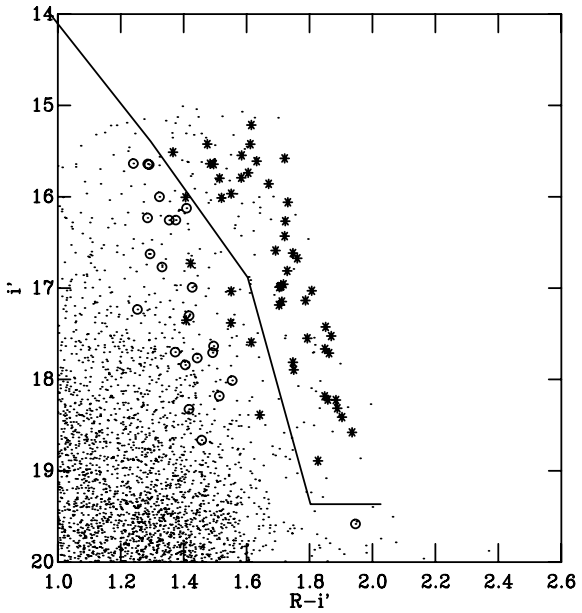


**Figure 1.** The CMD for the second epoch $Ri'$ catalogue. Spectroscopic members of Kenyon et al. (2005) and Burningham et al. (2005) are shown as asterisks. Objects identified as non-members in the same studies are shown as open circles. The solid line indicates the location of the cut for our PMS selection.

absorption, evidence of low surface gravity and the appropriate radial velocity.

To test if the observed C–M spread is affected by variability, we have assumed a single age for the young group and then simulated the PMS using an estimate of each object's variability, derived from our two-epoch observations. This method implicitly includes the effect of photometric uncertainty.

To verify that our PMS selection is indeed more variable than the background, we have compared the rms of the differences between the two sets of observations for the background objects and for the PMS selection. To make such a comparison meaningful, we have restricted our sample to those $i'$ magnitudes where the uncertainties are small. In Fig. 2, we plot the uncertainty in the $R - i'$ differences (thus incorporating uncertainties from both epochs) against $i'$

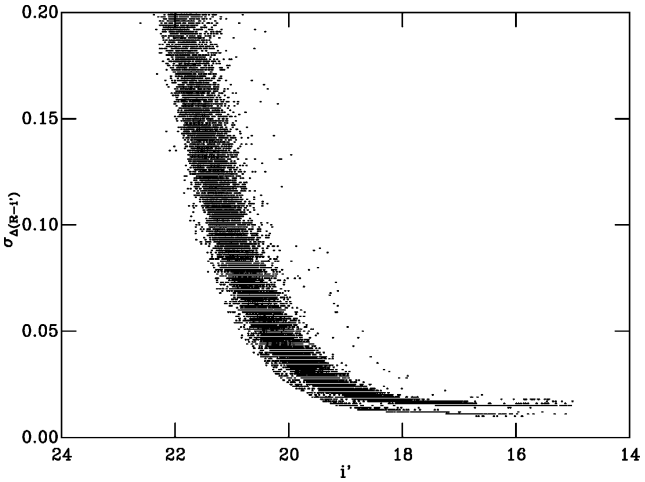


**Figure 2.** A plot of the uncertainty in $\Delta(R - i')$ against $i'$ for the FOV centred on the $\sigma$ Ori subgroup.

(second epoch). As can be seen, the uncertainties rise sharply fainter than $i' = 18$, as the uncertainty in the photon-counting statistics of the sky begins to dominate. Brighter than $i' = 16$, some objects also display higher uncertainties. This is because for these points that the first epoch data were drawn mainly from a short exposure. In the range $15 < i' < 18$, the uncertainties are dominated by the small magnitude-independent uncertainty measured during the normalization of the catalogues (see Naylor et al. 2002, and Section 2). Based on this plot, we restrict our comparison of the rms to the range $15 < i' < 18$. The rms of the differences between the two sets of observations indicates that the objects in the photometric PMS selection are significantly more variable than those in the background. The rms for the differences in $i'$ is 0.05 for the background and 0.09 for the PMS region. In $R - i'$, the rms is smaller: 0.02 for the background and 0.04 for the PMS region.

We placed the objects on a single empirical isochrone by fitting a third-order polynomial to the photometrically selected PMS in the CMD. Each point used for fitting the polynomial is weighted according to its uncertainty in $R - i'$, with the points carrying the greatest uncertainty having the smallest influence on the fit. A point was then placed on this empirical isochrone at the appropriate magnitude for each PMS object. One can view this as moving each point in colour until it falls on the isochrone.

Having placed each point on the isochrone, we simulated the effect of binaries by splitting this empirical isochrone into a single star and an equal mass binary sequence. We did not assume a binary fraction, but rather simulated spreads with a range of fractions. For each binary fraction, we randomly selected that proportion of objects to be offset in magnitude by an amount equal to $0.75(1 - f_{\rm bin})$, and the rest by $0.75 - 0.75(1 - f_{\rm bin})$. This gave rise to a difference of 0.75 mag between the two sequences, as would be expected from equal mass binaries. We did not attempt to simulate $q < 1$ binaries as these would fall within the envelope bounded by our two sequences, and thus would not have a significant impact on the results of this investigation.

To simulate the effect of variability, we next moved each point by an amount in both magnitude and colour equal to $(\Delta/\sqrt{2})$, where $\Delta$ is the observed difference between the two observations for that point. Characterizing the variability in this manner for each object in turn has distinct advantages over parametrizing the scatter of the whole sample, as any correlations between $\Delta i'$ and $\Delta(R - i')$ have been included without any assumptions as to the source of the variability. Furthermore, any correlation of variability with magnitude has also been included, as has the influence of photometric uncertainty.

A further source of scatter that might influence the observed spread is differential reddening. We have neglected the effects of differential reddening in this simulation since the extinction towards $\sigma$ Ori is low, with a colour excess of just $E(B - V) = 0.05$ (Lee 1968). To select which binary fraction gave the best match to the data, and thus which one would be used for subsequent analysis, we constructed a $\chi^2_\nu$ estimate for each simulation by comparing a histogram of the residuals in $R - i'$ from the polynomial fit to the data, with a histogram of the residuals from a polynomial fit to the simulation. The histograms were all constructed in an identical manner: we placed the residuals in bins of width 0.05 mag starting at $-0.5$ and ending at $+0.5$. Because we used a random number generator to select the objects that make up the binary sequence, we ran each simulation 1000 times to obtain a mean value for $\chi^2_\nu$, thus reducing the noise for the determination of the most likely binary fraction. Fig. 3 shows a plot of mean $\chi^2_\nu$ against binary fraction. Clearly, there is no sharp minimum in the value of $\chi^2_\nu$, but a broad minimum is

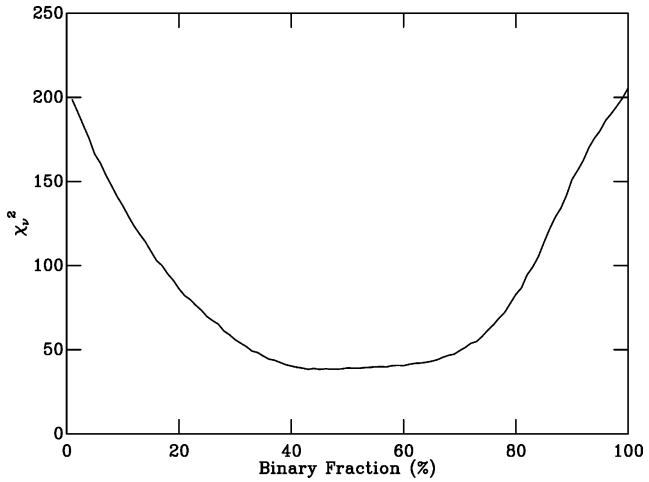


**Figure 3.** The mean $\chi^2_\nu$ for the simulated PMS compared to the observed PMS plotted against binary fraction, shown as a percentage for the PMS objects near $\sigma$ Ori.

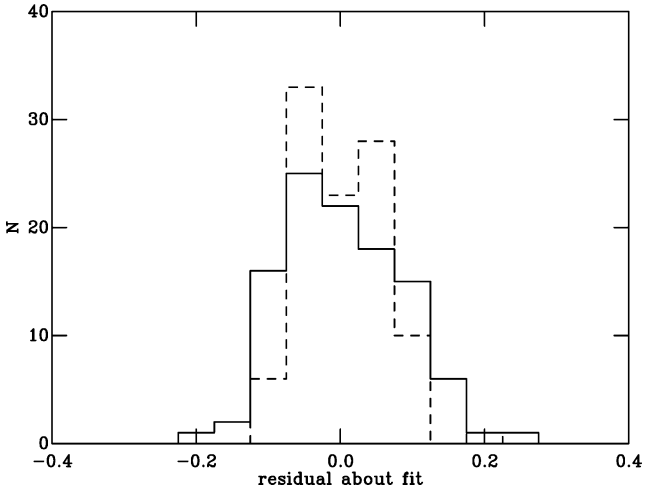


**Figure 5.** Histograms of the residuals in $R - i'$ about polynomial fits to the observed PMS (solid line) and the simulated PMS (dotted line) for the $\sigma$ Ori PMS sample (binary fraction 50 per cent).

centred on 50 per cent. We present one realization of the simulation for a binary fraction of 50 per cent in Fig. 4.

Comparison of panels (a) and (c) in Fig. 4 indicates that the combination of variability and binarity is not able to account for the spread in the PMS. In Fig. 5, we show histograms of the residuals about third-order polynomial fits to the observed PMS and the simulated PMS (solid and dotted line) for the $15 < i' < 18$ region of the CMD. Again, it is clear that the combination of binarity and variability on time-scales of $\sim$4 yr is not sufficient to explain the spread in the C–M space for this PMS. With such a poor match to the observed spread, it is clear why Fig. 3 displays no sharp minimum in $\chi^2_\nu$, but rather a broad minimum centred on 50 per cent. A binary fraction of 50 per cent maximizes the size of the spread, for a given estimate of variability. The assumption of a $q = 1$ binary population also increases the value of $\chi^2_\nu$ as it introduces a double peak to the spread which is not present in the data.

The full width at half-maximum of the spread in residuals in $(R - i')$ about the polynomial fit to the observed PMS, shown in Fig. 5, is approximately 0.3 mag. This is consistent with the width of the PMS observed by Sherry, Walter & Wolk (2004) in $V - i$ for more massive members of the same group.

### 3.2 Cep OB3b

In this case, we do not have the benefit of such a large spectroscopic sample as in the $\sigma$ Ori group. As a result, we have no estimate of the likely contamination from field stars, or the true extent of the PMS region in the C–M space. There have, however, been a number of studies that have identified likely low-mass members using a variety of techniques. Ogura, Sugitani & Pickles (2002) used H$\alpha$ spectroscopy to identify classical T-Tauri stars (CTTSs) in the vicinity of bright-rimmed clouds, and found 33 likely members of Cep OB3b, of which 16 are identified in our catalogue. Naylor & Fabian (1999) used *ROSAT* observations to identify 56 X-ray sources towards Cep OB3b using both High Resolution Imager (HRI) and Position Sensitive Proportional Counter (PSPC) observations. We have cross-correlated their X-ray catalogue with our optical catalogue, matching the brightest star within a radius of 14 arcsec for

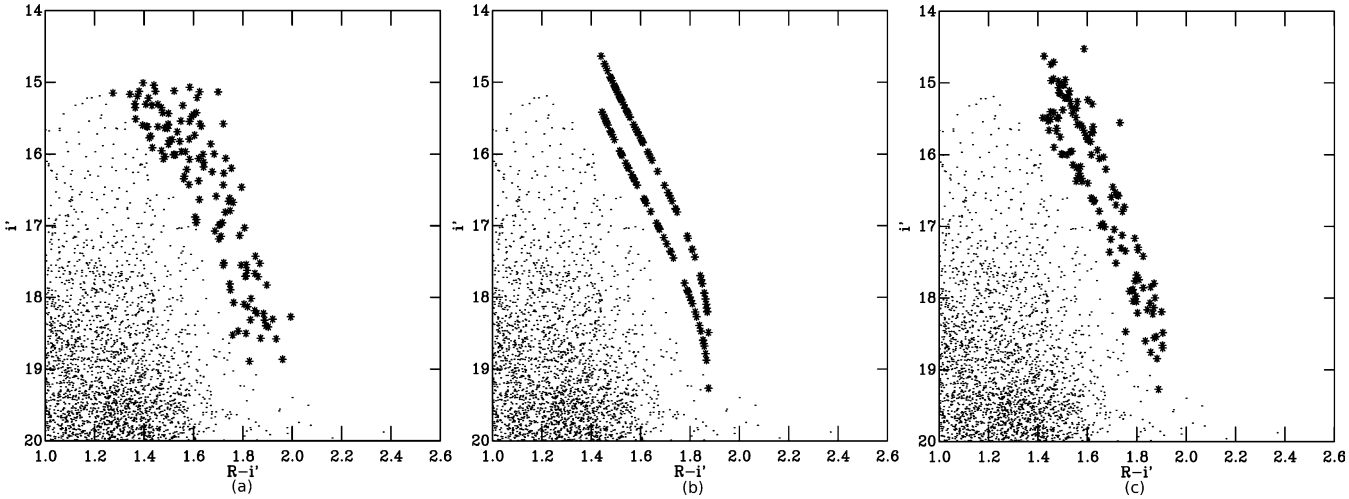


**Figure 4.** CMDs for the $\sigma$ Ori young group showing (a) the PMS selected objects as asterisks; (b) the fitted single star and binary sequences for a binary fraction of 50 per cent and (c) the simulated PMS for the same binary fraction.

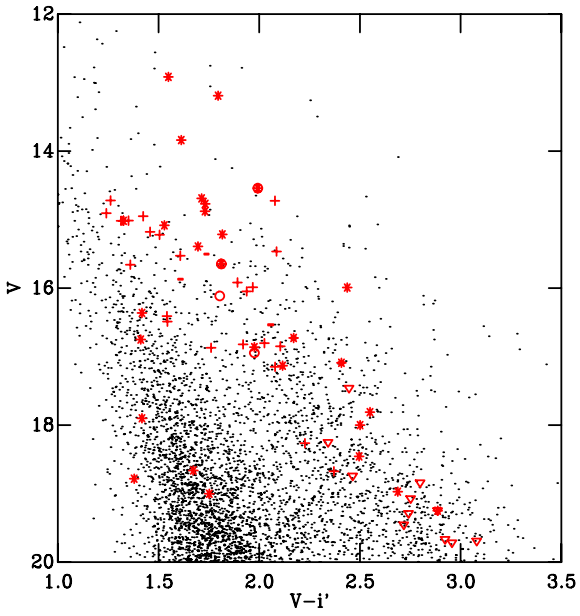


**Figure 6.** The CMD for the first epoch Cep OB3b data. Members identified by Ogura et al. (2002) are shown as open triangles, those from Naylor & Fabian (1999) are shown as asterisks, CTTSs from Pozzo et al. (2003) are shown as open squares, while the WTTSs are shown as open circles. Confirmed non-members from Pozzo et al. (2003) are shown as crosses. Those WTTS that were identified in both Naylor & Fabian (1999) and Pozzo et al. (2003) are shown as filled circles.

the PSPC positions and 7 arcsec for those from HRI. We find 21 PSPC objects correlate with objects in our catalogue, and 14 HRI objects. We reject all objects that lie in the Galactic background region on the left of the CMD from further use in this study as they are likely non-members (Burningham et al. 2005), identified by chance correlations with our catalogue. We accept as likely members those X-ray sources that correlate with objects in the expected PMS region of the $Vi'$ CMD shown in Fig. 6. Pozzo et al. (2003) used radial velocities and Li I absorption to identify both CTTSs and Weak T-Tauri stars (WTTSs) in Cep OB3b, and found five CTTS members and five WTTS members. Of these, all of the CTTSs and all-but-one of the WTTS are found in our catalogue. Pozzo et al. (2003) were also able to rule out membership for a number of objects and these are also indicated on the CMD. Fig. 6 shows the CMD for the first epoch data, with members from each survey overlaid, along with non-members from Pozzo et al. (2003). Since we are unable to make a reliable PMS selection beyond those members selected by previous authors, we simulate the photometric spread for these 49 likely members. Since more than half of our sample has been selected on the basis of X-ray activity, it might be argued that our sample is biased in favour of objects with the greatest rotational variability: WTTSs. On the other hand, WTTS variability is smaller in magnitude than non-periodic CTTS variability. As such, our simulation should still provide an indication of the contribution from variability to the observed spreads.

We have verified the variability of our member sample for Cep OB3b in the same manner as for the $\sigma$ Ori sample. Fig. 7 shows the uncertainty in the $(V - i')$ differences as a function of $V$ (first epoch). It is clear that the uncertainties start to increase dramatically fainter than about $V = 18$, and step up slightly at brighter than $V = 13$ for reasons similar to those described in Section 3.1. As such, we have calculated the rms for objects in the range of magnitudes $14 < V < 17.5$. The rms of the differences between the two sets

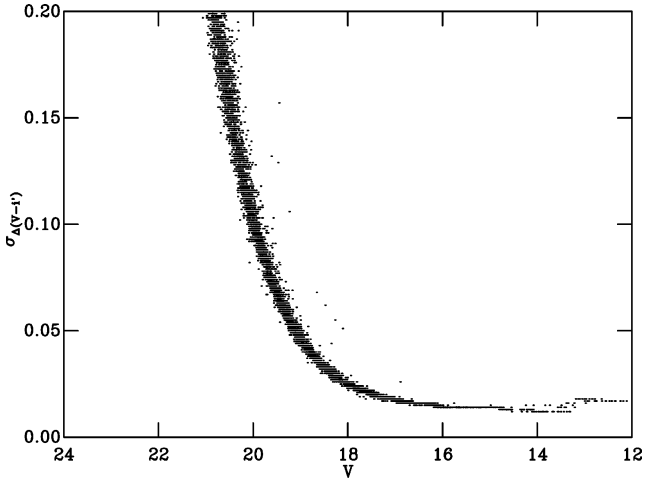


**Figure 7.** A plot of the uncertainty in $\Delta(V - i')$ against $V$ for the FOV in Cep OB3b.

of observations indicates that the likely members are significantly more variable than the rest of the sample. The rms of the differences in $V$ is 0.07 for the total sample, compared to 0.11 for the likely members. In $(V - i')$, the rms is smaller: 0.03 for the total sample and 0.07 for the likely members. A similar result is obtained if we attempt to make a photometric PMS selection. This indicates that a high proportion of objects in this region of the CMD may also be PMS members of Cep OB3b.

The member sequence was simulated in the same manner as the PMS sample in the previous section. As before, we were able to neglect the effect of differential reddening in our simulation, but for a different reason. Pozzo et al. (2003) found that the reddening vector in a $V/V - i'$ CMD lies nearly parallel to the PMS for sight-lines towards Cep OB3b. As such, the differential reddening is unlikely to add any spread to the observed sequence. The only difference between the two methods is that we have used a different bin size and range when constructing the histograms used for determining $\chi^2_\nu$. Because the sample size is smaller, we used a larger bin width (0.1), whilst extending the range of the bins ($-2.0$ to $+2.0$) to include some larger residuals. As can be seen in Fig. 8, a binary fraction of 25 per cent gives the closest match to the data.

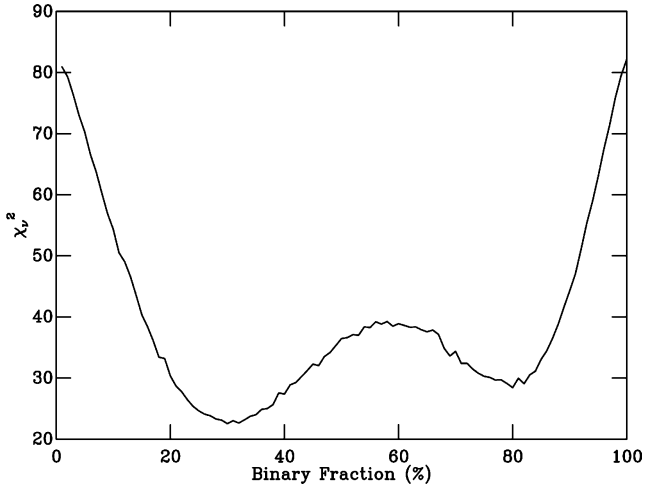


**Figure 8.** The mean $\chi^2_\nu$ for the simulated member sequence compared to the observed member sequence plotted against binary fraction, shown as a percentage for likely members of Cep OB3b.

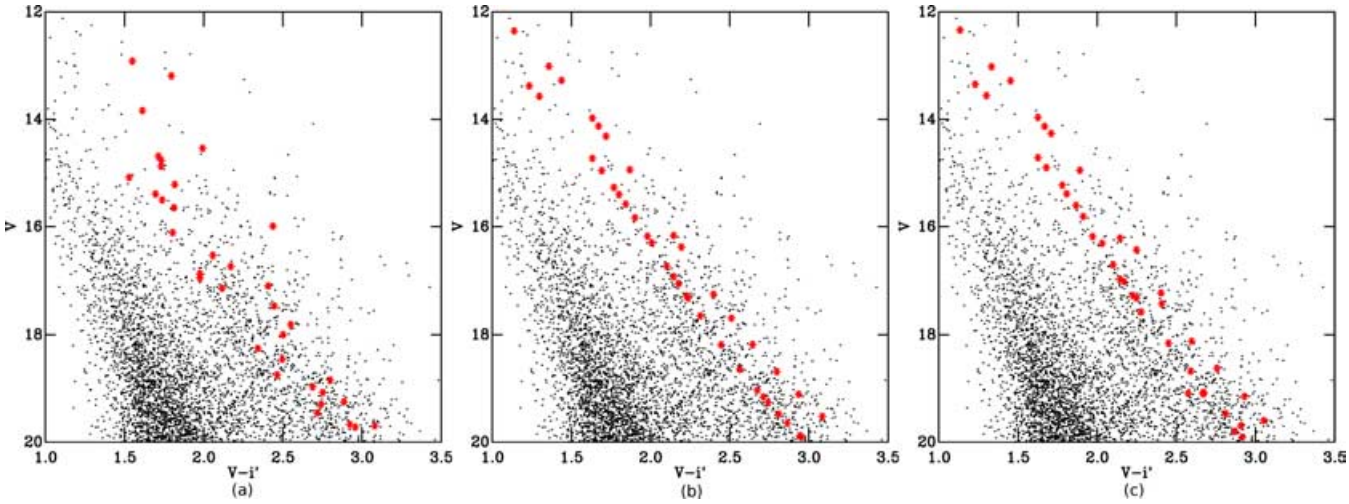


**Figure 9.** A CMD showing the fitted single star and binary member sequences as lines of red asterisks for a binary fraction of 0.25 for the Cep OB3b.

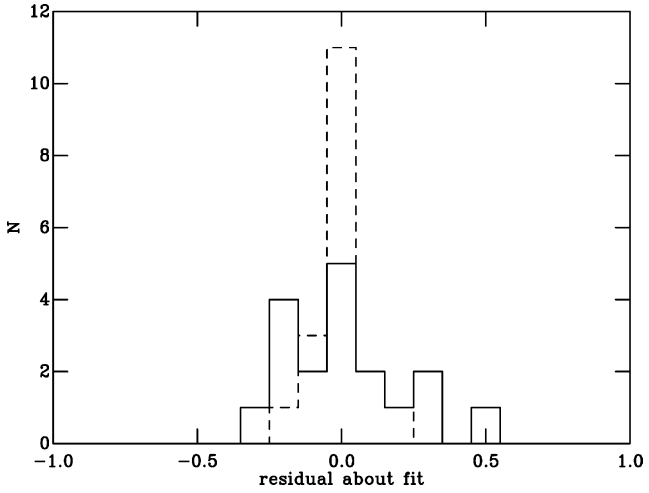


**Figure 10.** Histograms of the residuals in $V - i'$ about polynomial fits to the observed member sequence (solid line) and the simulated member sequence with a binary fraction of 25 per cent (dotted line) for Cep OB3b.

The fitted member sequence for this binary fraction is shown overlaid on CMD (b) in Fig. 9, whilst the simulated member sequence is shown on CMD (c) of the same figure. In Fig. 10, we have plotted a histogram of the residuals about the fit to the data and the simulation for the $14 < V < 17.5$ region of the member sequence for one realization of the simulation, using a binary fraction of 25 per cent. Inspection of Figs 9 and 10 indicates that, as was seen in the previous section for the $\sigma$ Ori young group, the combination of binarity and variability on a time-scale of $\sim$1 yr is not able to explain the spread of members in the C–M space.

## 4 DISCUSSION

We have shown that the photometric variability on time-scales of 1–4 yr is not able to account for the spread in the C–M space occupied by either of our sequences. If we assume that the influence of variability and binarity is added to the underlying distribution in quadrature, we can estimate the proportion of the observed spread that is accounted for here and that which remains unaccounted for. In the case of the $\sigma$ Ori young group, it appears that short-term variability can account for about half of the observed spread in the $Ri'$ C–M space. The rms of the residuals about the polynomial fit is 0.084 mag for the observed PMS, and 0.057 mag for the simulated sequence, which leaves 0.062 mag unaccounted for. Short-term variability can only account for about 1/20 of the spread in Cep OB3b, where the rms of the residuals about the polynomial fits is 0.20 mag for the observed member sequence, and 0.075 for the simulated sequence, leaving 0.185 mag unaccounted for.

### 4.1 The nature of the variability

Figs 11 and 12 show the measured differences in colour and magnitude for the objects in our final sample for each of our regions of interest. The distribution of C–M shifts is clearly different for the two regions, which is not surprising considering the different colours used for each case. The diagonal distribution of the Cep OB3b differences demonstrates that the variability seen here will

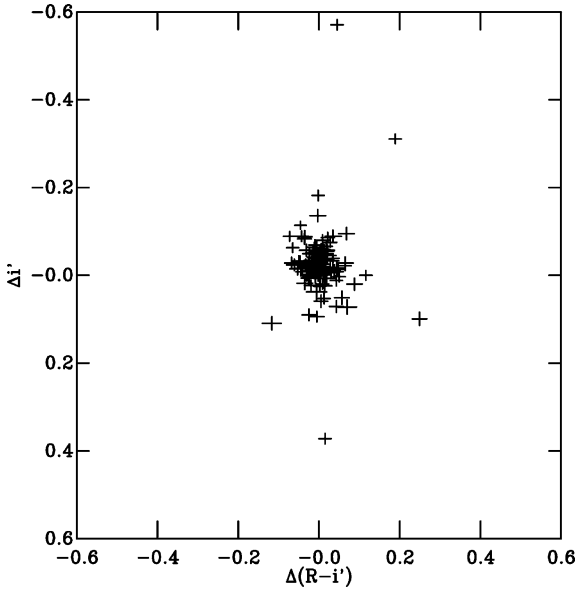


**Figure 11.** A plot of $\Delta i'$ against $\Delta(R - i')$ for the $15 < i' < 18$ region of the PMS in $\sigma$ Ori. The points are plotted with error bars.

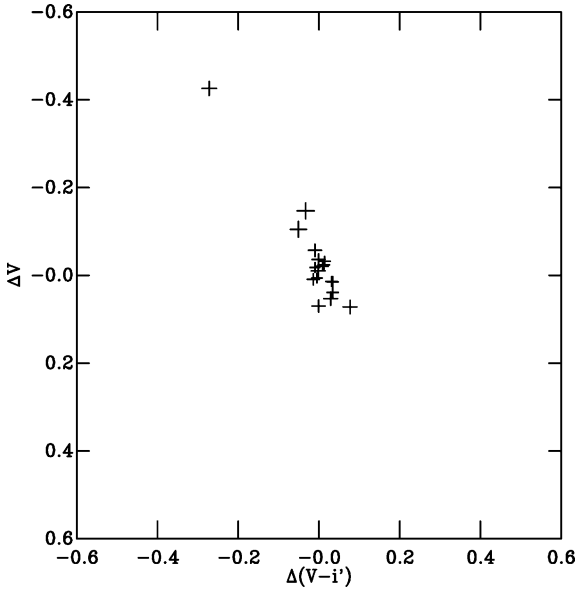


**Figure 12.** A plot of $\Delta V$ against $\Delta\,(V - i')$ for the $14 < V < 17.5$ region of the member sequence of Cep OB3b. The points are plotted with error bars.

only tend to move objects up and down an isochrone, and will have little impact on the apparent age spread. These differences, which indicate that objects get bluer when brighter, are consistent with variability arising from hot or cool spots on the surfaces of PMS stars rotating in and out of view. The differences shown in the plot for the $\sigma$ Ori subgroup display an uncorrelated distribution, which will tend to displace objects across isochrones more. As a result, the simulations carried out for this region display a greater apparent age spread. Since the $\sigma$ Ori observations are in $Ri'$, they are less sensitive to colour changes associated with rotational variability than $Vi'$ observations (Herbst et al. 1994), and so the different distributions of differences do not necessarily imply a different origin.

Our observations rule out variability on time-scales of 1–4 yr as the entire cause for the observed C–M spreads. The mechanisms this therefore excludes are rotation of hot or cool spots, and short time-scale non-periodic T-Tauri variability, such as that caused by accretion noise or chromospheric flaring. We can also rule out variability associated with the rotation of structures in the disc out to a radius of 1 au as a source for the C–M spread, since the rotation of such structures should occur within a year. It is also unlikely that rotation of bright structures beyond 1 au would be responsible for the C–M spread as the temperature in a thin disc drops rapidly with distance, such that at a radius of 1 au the temperature is $\sim$100 K. As such the outer disc is only likely to contribute appreciable flux in the far-infrared.

The rms of residuals about the polynomial fit to the simulated PMS is larger in Cep OB3 than in the $\sigma$ Ori young group. Since accreting objects are known to be more variable than non-accreting objects, this is consistent with the observed incidence of accretors in the two regions. Kenyon et al. (2005) found the fraction of low-mass accretors to be $10 \pm 5$ per cent in the $\sigma$ Ori young group, whilst the small number of members identified by Pozzo et al. (2003) in Cep OB3b suggests about 50 per cent of objects there are accretors.

Since longer time-scale variability may be the origin of the remaining unexplained spread, we cannot confirm the reality of the apparent age spreads. However, what is clear is that the actual size of either age spread is smaller than that observed, and possibly zero. Returning to the rms of the residuals about the polynomial fits, we recall that the unaccounted for spread has an rms of residuals about the fit of 0.062 mag in the case of the $\sigma$ Ori subgroup, and 0.185 mag in the case of Cep OB3b.

It is tempting to read much into the observation that the larger remaining spread is seen in the association whose natal molecular cloud would have had the larger crossing time. However, it should be noted that in the case of the $\sigma$ Ori subgroup the apparent spread, and thus the underlying one also, may be larger since we were conservative in our PMS selection. As can be seen in Fig. 1, we have actually excluded some members in order to avoid risking significant contamination by non-members in our photometric selection. The excluded members have the same mean variability as the members that were selected, so the simulated spread has not been altered significantly by their exclusion.

Although we are confident that our selection is not subject to significant contamination (see Burningham et al. 2005; Kenyon et al. 2005), there will, none the less, be some non-members included in the sample. These objects will not increase the size of the observed spread since our confirmed members span the entire selected region of the CMD (see Fig. 1). However, it is likely that they will reduce the rms of residuals about the polynomial fit to the simulated spread, as any non-members can be expected to be less variable than the members. If this is the case, then it may still be that the remaining unexplained spread in the $\sigma$ Ori is very small.

It is still possible that the C–M spreads arise as a result of some other kind of photometric variability. Such variability could arise from variations in accretion flow caused by stellar magnetic cycles (e.g. Armitage 1995), with time-scales of a few years to decades. Alternatively, much longer time-scale variability such as that resulting from accretion-driven age spreads could be to blame. Fundamentally, the influence of such long-term accretion processes on the presence of apparent age spreads would be best determined through a study of accretion rates across a large number of objects in associations that display a range of apparent spreads, rather than a longer baseline variability study.

### 4.2 Apparent age spread and absolute age

As was briefly discussed out in Section 1.3, the size of age spread inferred from a given photometric spread depends on the median age of the star-forming region in question. This should be borne in mind when interpreting any unexplained spread in terms of an age spread. For example, consider the $\sigma$ Ori young group. If we accept an age of 5 Myr and a distance of 350 pc, as we did in Burningham et al. (2005), then the remaining $R - i'$ spread of 0.062 mag represents a spread of approximately 4 Myr (3.5–7 Myr), based on the separation of NextGen isochrones (Chabrier & Baraffe 1997; Baraffe et al. 2002) at $i' = 16.5$. If on the other hand we adopt the age found by Sherry et al. (2004) of 2.5 Myr and the distance they used for that estimate, 440 pc, we find the remaining $(R - i')$ spread corresponds to an age spread of approximately 2 Myr (2–4 Myr).

In the case of the Cep OB3b association, Pozzo et al. (2003) found the ages of PMS objects to range from $<$1 Myr to nearly 10 Myr using isochrones laid on to a $V/V - i$ CMD. As has been shown here, variability and binarity can only account for a small fraction of this spread.

## 5 CONCLUSIONS

We have used two-epoch, two-colour photometry to investigate the influence of photometric variability on the apparent age spreads in

CMDs. We have found that the combination of binarity and variability on time-scales of $\sim$ years cannot account for the observed spread in the C–M space. We argue that the remaining unexplained spread must reflect either a genuine spread of ages or longer time-scale variability associated with the changes in the accretion flow on to the PMS objects.

## REFERENCES


Armitage P. J., 1995, MNRAS, 274, 1242
Ballesteros-Paredes J., Hartmann L., Vázquez-Semadeni E., 1999, ApJ, 527, 285
Baraffe I., Chabrier G., Allard F., Hauschildt P. H., 2002, A&A, 382, 563
Burningham B., Naylor T., Jeffries R. D., Devey C. R., 2003, MNRAS, 346, 1143
Burningham B., Naylor T., Littlefair S. P., Jeffries R. D., 2005, MNRAS, 356, 1583
Chabrier G., Baraffe I., 1997, A&A, 327, 1039
Dolan C. J., Mathieu R. D., 2001, AJ, 121, 2124
Elmegreen B. G., 2000, ApJ, 530, 277
Hartmann L., 2001, AJ, 121, 1030
Hartmann L., 2003, ApJ, 585, 398
Hartmann L., Ballesteros-Paredes J., Bergin E. A., 2001, ApJ, 562, 852
Herbst W., Miller D. P., 1982, AJ, 87, 1478
Herbst W., Herbst D. K., Grossman E. J., Weinstein D., 1994, AJ, 108, 1906
Jijina J., Myers P. C., Adams F. C., 1999, ApJS, 125, 161
Kenyon M. J., Jeffries R. D., Naylor T., Oliveira J. M., Maxted P. F. L., 2005, MNRAS, 356, 89
Lee T. A., 1968, ApJ, 152, 913
Littlefair S. P., Naylor T., Burningham B., Jeffries R. D., 2005, MNRAS, 358, 341
Mac Low M., Klessen R. S., 2004, Rev. Mod. Phys., 76, 125
Naylor T., 1998, MNRAS, 296, 339
Naylor T., Fabian A. C., 1999, MNRAS, 302, 714
Naylor T., Totten E. J., Jeffries R. D., Pozzo M., Devey C. R., Thompson S. A., 2002, MNRAS, 335, 291
Ogura K., Sugitani K., Pickles A., 2002, AJ, 123, 2597
Palla F., Stahler S. W., 2000, ApJ, 540, 255
Palla F., Stahler S. W., 2002, ApJ, 581, 1194
Pozzo M., Naylor T., Jeffries R. D., Drew J. E., 2003, MNRAS, 341, 805
Pringle J. E., Allen R. J., Lubow S. H., 2001, MNRAS, 327, 663
Sherry W. H., Walter F. M., Wolk S. J., 2004, AJ, 128, 2316
Shu F. H., 1977, ApJ, 214, 488
Shu F. H., Adams F. C., Lizano S., 1987, ARA&A, 25, 23
Sung H., Bessell M. S., Lee S., 1998, AJ, 115, 734
Tassis K., Mouschovias T. C., 2004, ApJ, 616, 283
Tout C. A., Livio M., Bonnell I. A., 1999, MNRAS, 310, 360
Ward-Thompson D., Scott P. F., Hills R. E., Andre P., 1994, MNRAS, 268, 276


This paper has been typeset from a TEX/LATEX file prepared by the author.